frontiers | Frontiers in Earth Science

TYPE Original Research
PUBLISHED 12 January 2023
DOI 10.3389/feart.2022.1052734

OPEN ACCESS

EDITED BY
Shuai Yin,
Xi'an Shiyou University, China

REVIEWED BY
Teng Zhao,
China University of Geosciences, China
Xiaowei Lv,
Chengdu University of Technology, China

*CORRESPONDENCE
Haihua Zhu,
zhhswpu@163.com

SPECIALTY SECTION
This article was submitted to Structural Geology and Tectonics, a section of the journal Frontiers in Earth Science

RECEIVED 24 September 2022
ACCEPTED 28 December 2022
PUBLISHED 12 January 2023

CITATION
Zhang R, Zhang B, Wang M, Zhu H, Zhang S, Tang W, Zhou H, Li Y, Bai R, Jia M, Zhu Y and Han L (2023), Paleo-sedimentary environment and lithofacies of Jurassic Da'anzhai Member in the Central Sichuan Basin-A case study of Well Ren'an 1.
Front. Earth Sci. 10:1052734.
doi: 10.3389/feart.2022.1052734

Paleo-sedimentary environment and lithofacies of Jurassic Da'anzhai Member in the Central Sichuan Basin-A case study of Well Ren'an 1

Rui Zhang[1,2], Benjian Zhang[2], Minglei Wang[3], Haihua Zhu[4,5]*, Shaomin Zhang[2], Wenqiang Tang[2], Hongfei Zhou[2], Yucong Li[2], Rong Bai[2], Min Jia[2], Yiqing Zhu[2] and Luyuan Han[2]

[1]Key Laboratory of Exploration Technologies for Oil and Gas Resources, Ministry of Education, Yangtze University, Wuhan, China, [2]PetroChina Southwest Oil & Gas Field Company, Chengdu, China, [3]PetroChina Research Institute of Petroleum Exploration & Development, Beijing, China, [4]School of Geoscience and Technology, Southwest Petroleum University, Chengdu, China, [5]The Unconventional Reservoir Evaluation Department, PetroChina Key Laboratory of Unconventional Oil and Gas Resources, Chengdu, China

The Jurassic Da'anzhai Member in Sichuan Basin is an important target for shale oil exploration. Whole rock X-ray diffraction analysis, thin section, SEM and TOC testing, as well as major and trace element analysis are used to analyze the relationship of lithofacies and pore types with the sedimentary environment of the Da'anzhai Member in the Central Sichuan Basin. The results show the Da'anzhai Member in the Well Ren'an 1 (RA1) is divided into six types of lithofacies, based on a three-level division method of mineral composition-TOC-mineral structure— namely, massive mud-bearing shell limestone lithofacies (F), thick argillaceous shell limestone lithofacies (E), laminated clay silt shale lithofacies (D), thin shell calcareous shale lithofacies (C), laminated shell-bearing shale lithofacies (B), and thick clay shale lithofacies (A). The pore spaces include intergranular pores, intergranular dissolution pores, authigenic calcite intergranular pores, authigenic quartz intercrystalline pores, intergranular pores of clay minerals or pyrite nodules, as well as organic pores. The Da'anzhai Member was deposited in a semi-deep to shallow lake sedimentary environment, with relatively low salinity. This strata experienced moderate-to-strong chemical weathering as a result of the semi-arid, warm and humid paleoclimate environmental conditions that persisted during its deposition; low weathering and dry paleoclimate conditions occurred periodically. Paleoenvironment is an important influence on the lithofacies and pore types of the Da'anzhai Member. The persistence of arid climate conditions contributed to a decline in water depth, relatively high salinity, low organic productivity, and the deposition of carbonate rocks that characterize lithofacies E and F; mostly intercrystalline pores formed in these lithofacies in response to the prevailing arid climate conditions. Conversely, warm, and humid climate conditions increased the inflow of fresh water, terrigenous debris, and nutrients into the lacustrine basin that led to the deposition of fine-grained sedimentary rocks of lithofacies A, B, and C. These lithofacies are characterized by abundant nano pores, such as clay intercrystalline pores and organic pores.

KEYWORDS

lithofacies, shale, sedimentary environment, Da'anzhai Member, Central Sichuan Basin

1 Introduction

The Sichuan Basin, located in the northwest Yangtze Platform, covers an area of about 19 $km^2 \times 10^4$ km^2. It is a typical multi-stage tectonic superposition basin, and the oil and gas source rocks in the Sichuan Basin are thick and widely distributed (Liu et al., 2012). Previous studies on the shale formations of the Da'anzhai Member are few, and mainly focus on their stratigraphy, lacustrine shale sedimentary facies, organic matter abundance, formation of source rocks, and hydrocarbon generation potential (Yang et al., 2005; Zheng, 2014; Chen et al., 2015). Paleo-environmental studies focus on basin evolution during the Silurian and Triassic (Wang et al., 2016; Zhou et al., 2021). A previous study on the sedimentary paleo-environment of the Da'anzhai section in Central Sichuan suggests the presence of a brackish—fresh water environment, characterized by moist and anoxic reduction (Lei et al., 2021).

Various types of lithofacies are recognized in the Da'anzhai Member. Wang C. Y et al. (2022) classified 17 lithofacies and five fine-grained sedimentary facies assemblages in the Yuanba area of the Sichuan Basin. However, the relationship between paleoenvironment and lithofacies and pore types of the Da'anzhai Member is rarely discussed.

Shale is a typical fine-grained sedimentary rock and an important carrier of hydrocarbon molecules (Curtis, 2002; Li et al., 2019; Li et al., 2022; Meakin et al., 2013; Su et al., 2018; Zhu et al., 2018; Zou et al., 2010). Its mineral composition, major and trace elements, as well as type and abundance of organic matter are closely related to the sedimentary environment and climate conditions at the time of deposition (Fu et al., 2018; Huo et al., 2022; Milliken, 2014). Studying these factors typically employs laboratory-based measurements of major and trace element geochemistry, organic geochemistry biomarkers, rare Earth element geochemistry, and isotope geochemistry (Gao et al., 2020).

In this paper, the lithofacies types, paleoclimate, paleo-water depth, paleo-productivity, paleo-redox environment, paleo-productivity, and the control of sedimentary environment on lithofacies in the Da'anzhai Member are studied from samples of Well RA1, in the Longgang area of the Central Sichuan Basin, using thin sections, X-ray diffraction (XRD), and elemental geochemical experiments.

2 Geological background

The study area is located in the Renhe Gentle Tectonic Belt which is a part of the Central Sichuan Gentle Fold Area (Figure 1) (Huang et al., 2018). Its tectonic evolution was controlled mainly by the rigid basement of the Qinling Mountains and the Sichuan Basin; some gentle, low hill-like anticlines were developed in this area. Drilling data suggests that the Da'anzhai Member, which is the focus of this study, is 70–100 m thick; gray-brown limestone, gray-black shale, and gray-brown limestone are developed within this member. It is divided into the Da 3, Da 2, and Da 1 sub-members, from bottom to top. Medium and thick, massive shell limestone intercalated with shale are developed in the Da 1 sub-member; gray-black and black shale interbedded with gray-black shale and gray-brown limestone are developed in the Da 2 sub-member; and massive shell limestone are developed in the Da 3 sub-member (Xiao et al., 2021).

The Da'anzhai Member of the Ziliujing Formation is an integrated contact with both, the overlying transition layer and the underlying Ma'anshan Formation. Its depositional period marks a period of time when the regional extension regime was at its weakest; orogen activity was the most stable during this period. The depression rate of the whole Sichuan Basin was higher as compared to the accumulation rate of terrigenous debris. Furthermore, the largest lake basin in the Early Jurassic was formed here A significant part of the Da'anzhai Member in the study area formed as part of a semi-deep lake—deep lake sedimentary facies deposition. A lacustrine transgression occurred during the depositional period of the Da 3 sub-member, and the largest lake basin was formed during the Da 2 sub-member stage.

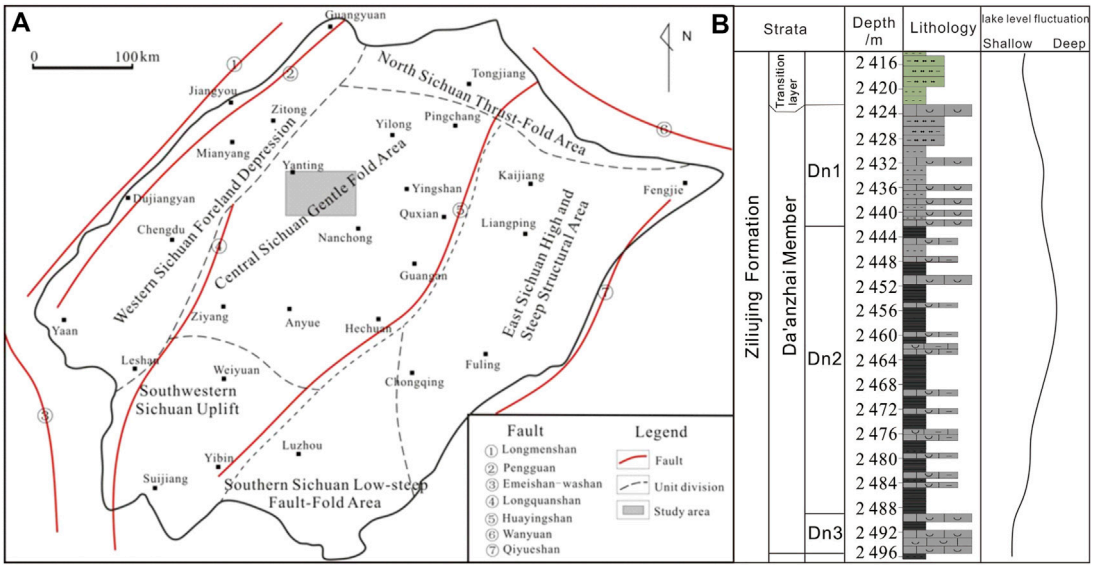

FIGURE 1
(A) Regional geology map of the Sichuan Basin marking the study area and **(B)** the stratigraphic column of the Da'anzhai Member of the Ziliujing Formation.

Lacustrine regression occurred during the late stage of deposition of the Da 2 sub-member. By the late stage of sedimentation of the Da 1 sub-member, the lake had dropped to a lower level and shell limestones are well developed here (Li and He, 2014).

3 Samples and methods

Fifty-six samples, collected from the Da'anzhai Member of Well RA1 at depths ranging from 2,432.26 to 2,485.13 m, are used in this study. All samples, pulverized to 200 mesh size powder, were split into several parts for analysis, including whole-rock X-ray diffraction (XRD), organic carbon and major and trace elements testing.

TOC content was determined by the combustion method of Krom and Berner (1983); measurements were done with a LECO-230 carbon and sulfur analyzer. Samples were treated with hydrochloric acid to remove carbonates prior to measurement. The reproducibility of TOC measurements is better than .1%.

Mineral compositions were analyzed by the X-ray diffraction (XRD) method using a D/Max 2500 PC type powder X-ray diffractometer. Standard powder diffraction data provided by the Consortium International Data Center for Powder Diffraction (JCPDS-ICDD) was used as a standard. The whole-rock mineral content in the shale samples was calculated by the K-value method.

An AxiosMAX XRF was used for X-ray fluorescence spectrometry to measure the oxides of major elements, including SiO_2, Al_2O_3, CaO, K_2O, Na_2O, Fe_2O_3, MnO, MgO, TiO_2, and P_2O_5. Analytical procedures were in accordance with Chinese National Standard GB/T 14506.28-2010, and the FeO was analyzed according to GB/T 14506.14-2010. The precision of the major element data is ≤3%.

An inductively coupled plasma mass spectrometer (ICP-MS PE300D) was used to determine the trace element contents in accordance with GB/T 14506.30-2010. For all samples, a fixed volume (40 mg) was first toasted in an oven at 105°C for 1–2 h and cooled to room temperature, then digested with 2.5 mL HF and .5 mL HNO_3 in a tightly sealed Teflon screw–cap beaker at 190°C for 24 h, and then dried. The dried sample was dissolved again in 5 mL 30% (v/v) HNO_3 for 3 h at 130°C and diluted to 25 mL before testing. The lower detection limit for elements was $0.n \times 10^{-12}$–$n \times 10^{-12}$(n = 1–9).

4 Results

4.1 Lithofacies type

The three-level lithofacies division method of mineral composition-TOC-mineral structure (Michaelis et al., 2002) are used to divide the lithofacies of the Da'anzhai Member in Well RA1. Main components of the fine-grained sedimentary rocks in the target layer include calcite, clay, and quartz, followed by dolomite and feldspar. The content of calcite ranges from 5.0% to 56.1%, with an average of 18.5%; the clay minerals are mainly illite, with a content of 35%–49%, with an average of 42%; the content of quartz varies between 6.12% and 51.57%, with an average of 33.7%. Of these minerals, most of the clays and quartz come from the weathering of rocks at the edge of the basin; they are physically transported into the lake basin. The calcite is mostly formed by bio-chemical precipitation in the basin. Due to the difference in their origins, both clay minerals and quartz showed a significant negative correlation with carbonate components (Figure 2).

The internal composition of the rock can reflect its environment of development. Felsic, clay and carbonate minerals are the end members in a triangle diagram, where their content is capped at 50% (Figure 3). Four rock categories are defined here: siltstone, clay rock, carbonate rock, and mixed fine-grained rocks. Organic matter plays an important role in oil and gas generation, in diagenesis, as well as in organic pore evolution (Fu et al., 2018; Zhou et al., 2020). Therefore, organic matter abundance should be considered when classifying shale facies types. Statistics show that the organic matter abundance (TOC) of the Da'anzhai section is low, with TOC ranging from .6% to 3.16%, with an average of 1.27%. The lower limit of TOC for the Da'anzhai shale oil reservoirs is 1.5%. The lower content of TOC (0%–1.5%) means that the Da'anzhai section is largely poor in organic matter, except for where a locally higher content of TOC (>1.5%) signals an enriched organic zone.

Based on a comprehensive consideration of mineral content, organic matter abundance, and sedimentary structures, the Da'anzhai Member of Well RA1 is divided into six lithofacies: massive mud-bearing shell limestone, Lithofacies F; thick argillaceous shell limestone, Lithofacies E; laminated clay silt shale, Lithofacies D; thin shell calcareous shale, Lithofacies C; laminated shell-bearing shale, Lithofacies B; and massive siliceous shale, Lithofacies A (Figure 3).

4.1.1 Massive siliceous shale (Lithofacies A)

The mineral debris is mainly mud grade with silt debris scatter distributed in massive mud-bearing shell limestone lithofacies (Figure 4). Clay minerals are cryptocrystalline and have microscopic scale-like structures. Organic matter is scattered in the form of spots, and in short thin strips. The average content of felsic minerals, clay minerals, carbonate components, and TOC were 40.15%, 50.61%, 9.24%, and 1.578%, respectively.

4.1.2 Laminated shell-bearing shale (Lithofacies B)

Mainly argillaceous structures are mainly developed in the laminated shell-bearing shale lithofacies (Figure 4B). Small amounts of silt and shell debris are distributed in short, thin strips. Clay minerals are cryptocrystalline and have microscopic scale-like structures. Organic matter is scattered in spots and short, thin strips. The average content of felsic minerals, clay minerals, carbonate components, and TOC were 43.29%, 43.23%, 13.48%, and 1.41%, respectively.

4.1.3 Thin shell calcareous shale (Lithofacies C)

Clay minerals are well developed in this thin shell calcareous shale lithofacies (Figure 4C). They have a cryptocrystalline structure, and lamellar oriented shells are visible. Organic matter is distributed as spots and in short, thin strips. The average content of felsic minerals, clay minerals, carbonate components, and TOC were 37.68%, 39.45%, 22.87%, and 1.33%, respectively.

4.1.4 Laminated clay silt shale (Lithofacies D)

Muddy laminae and granular laminae are developed within the laminated clay silt shale lithofacies (Figure 4D). These structures are mainly composed of cryptocrystalline clay minerals and terrigenous silt, and the silt components in some samples have directional distribution characteristics. The average content of felsic minerals, clay minerals, carbonate components, and TOC were 34.75%, 40.33%, 18.49%, and 1.29%, respectively.

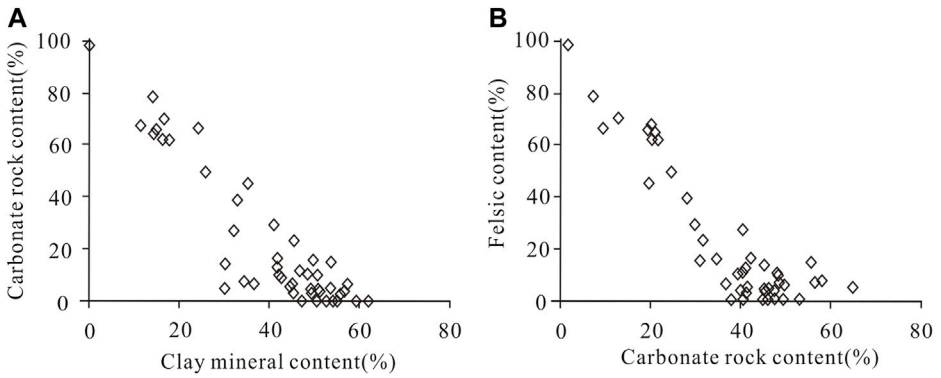

FIGURE 2
(A) Relationship between carbonate and clay minerals and **(B)** carbonate minerals and felsic components in the target layer of Well RA1.

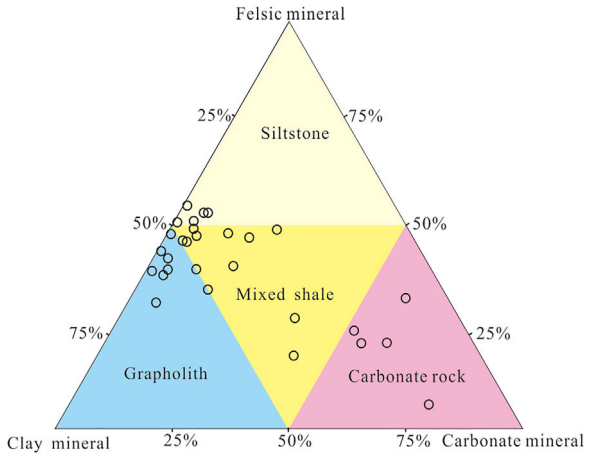

FIGURE 3
Triangular mineral composition diagram of Well RA1.

4.1.5 Medium-thick argillaceous shell limestone (Lithofacies E)

The sedimentary structure of the medium-thick argillaceous shell limestone lithofacies is massive (Figure 4E). Its main lithology is shell limestone with argillaceous components. The average content of felsic minerals, clay minerals, carbonate components, and TOC were 31.22%, 26.73%, 42.03%, and 1.15%, respectively.

4.1.6 Massive mud-bearing shell limestone (Lithofacies F)

Shell limestones are developed in massive mud-bearing shell limestone facies (Figure 4A). The average content of felsic minerals, clay minerals, carbonate components, and TOC were 41.36%, 35.78%, 22.85%, and 1.04%, respectively.

4.2 Pore structure features

Many pore types are identified in the Da'anzhai Member; karst caves, fractures, dissolution pores, and intercrystalline pores were reported from the shell limestones (Pang et al., 2018); fractures, organic pores, and inorganic pores were reported from the shales (Zhu et al., 2022). In this paper, the pores of the Da'anzhai Member are divided into two types, inorganic and organic pores. Inorganic pores are further divided into six subtypes, according to their mode of origin and distribution. Of these, the intercrystalline pores in shell calcite are distributed within the large shell (Figure 5A). The pores that formed during the recrystallization process of the shell are polygonal, with straight and regular edges; they have large pore diameters. The process of shell recrystallization may be accompanied by dissolution, resulting in the formation of intercrystalline dissolution pores in shell calcite. These pore edges are typically smooth (Figure 5B).

Intercrystalline pores of authigenic calcite refer to the intercrystalline pores within the calcite cement (Figure 5C). They are mostly distributed between the shells or in the early shielding space formed by them. In the diagenetic process, shell calcite is easily replaced by quartz, and a large number of quartz intercrystalline pores can form within the authigenic quartz (Figure 5D). Clay intercrystalline pores are the most common, which are distributed among platelet clay minerals (Figure 5E). They usually occur as flakes, in large numbers, and with small pore sizes. Microscopic observations show that their pore sizes range from 5 to 550 nm, with peak distribution between 50 and 99 nm. Intergranular pores of pyrite refer to the pores between authigenic pyrite crystals (Figure 5F), which are filled either completely or partly with organic matter; they are unevenly distributed and have weak local connectivity. Organic pores are distributed in amorphous asphaltene bodies (Figures 5G, H), and the degree of development is low. Pores in kerogen are rare. Pores in organic matter are small and round, with pore size mainly distributed from 0 to 149 nm, with peak distribution at 55–99 nm.

5 Discussion

The content of major and trace elements in sedimentary rocks can be used to characterize the water media and paleoclimate changes during the formation of the strata (Wang et al., 2019). This is because the physical and chemical properties of the elements, and the paleoclimate have a tremendous influence on the distribution of elements (McLennan et al., 1993; Nesbitt and Young, 1989). The geochemical properties of elements are complex. The adsorption of specific mineral particles to specific elements, the exchange of

FIGURE 4
Photographs of cores showing the developmental characteristics of different lithofacies in Well RA1; **(A)** massive mud-bearing shell limestone, Lithofacies F, 2,435.28–2,435.45 m; **(B)** laminated shell-bearing shale, Lithofacies B, 2,466.94–2,466.97 m; **(C)** thin shell calcareous shale, Lithofacies C, 3,496.51–3,496.68 m; **(D)** laminated clay silt shale, Lithofacies D, 2,466.84–2,466.97 m; **(E)** medium-thick argillaceous shell limestone, Lithofacies E, 2,459.19–2,459.27 m; **(F)** massive mud-bearing shell limestone, Lithofacies F, 2,466.31–2,466.84 m.

elements between sediments and aqueous media, the chemical properties of the elements themselves, and the paleoenvironment all affect the distribution of elements. Elemental geochemical indicators can, under different sets of conditions, offer limited interpretations of the sedimentary environment. For example, redox-sensitive trace elements can be used to characterize redox conditions only when they are concentrated from the water body, rather than from terrigenous detritus. In this study, the poor correlation of these redox-sensitive trace elements with Th indicate that U, V, Ni, and Cr in the sediments concentrated through authigenic enrichment rather than from detrital input (Figure 6).

5.1 Paleoclimate evaluation

In sedimentary environments, with stable tectonic activity, climate has significant influence on the depositional environment; it controls the temperature, Eh, pH, and paleosalinity. Common indicators used to describe paleoclimate conditions include the paleoclimate index (*C*), Sr, Cu and Sr/Cu, Fe/Cu, Mg/Ca, Fe/Mn, and SiO_2/AlO_3. In this study, the chemical index of alteration (*CIA*) and climate index (*C*) were used to analyze the paleoclimate conditions prevalent at the time of formation of the Da'anzhai Member. Paleoclimate and parent rock composition can affect the weathering intensity, and *CIA* is an effective indicator parameter of paleoclimate. Following Fu et al. (2017), CIA is calculated as

$$CIA = 100 \times Al_2O_3 / (Al_2O_3 + CaO + Na_2O + K_2O) \quad (1)$$

A larger chemical index of alteration (*CIA*) indicates stronger chemical weathering influenced by a relatively warm and humid climate. Generally, elements such as Fe, Mn, V, Cr, Ni, Co are easily enriched in sedimentary rocks under wet conditions. However, in a dry environment, the evaporation of water enhances the alkalinity in the water body; as a result, basic metal ions such as Na, K, Ca, Mg, Sr, Ba are accumulated in the sediments. The ratio of the above-mentioned types of elements can be used to evaluate the paleoclimate. In this study, the climate index (*C*) and the chemical index of alteration (*CIA*) were used to study the paleoclimate of the

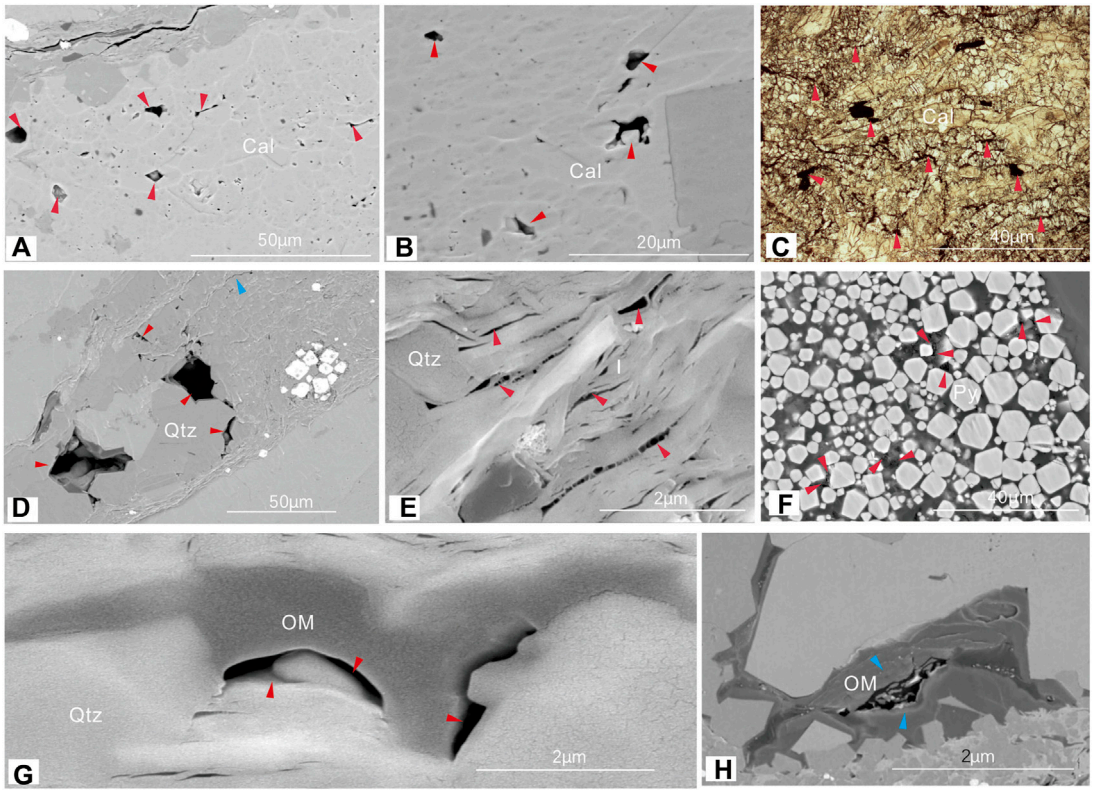

FIGURE 5
Photomicrographs of shale reservoirs in the Da'anzhai Member in Well RA1; **(A)** intergranular pores in shell calcite, 2,453.13 m; **(B)** intergranular dissolution pores in shell calcite, 2,453.13 m; **(C)** authigenic calcite intergranular pores (red arrow), 2,449.94 m; **(D)** authigenic quartz intercrystalline pores and shell edge fractures, 2,461.05 m; **(E)** intergranular pores of clay minerals, 2,464.4 m; **(F)** intergranular pores of pyrite nodules, filled with organic matter, 2,464.4 m; **(G)** organic pores in asphaltenes, 2,449.94 m; **(H)** organic pores in asphaltenes, 2,451.23 m.

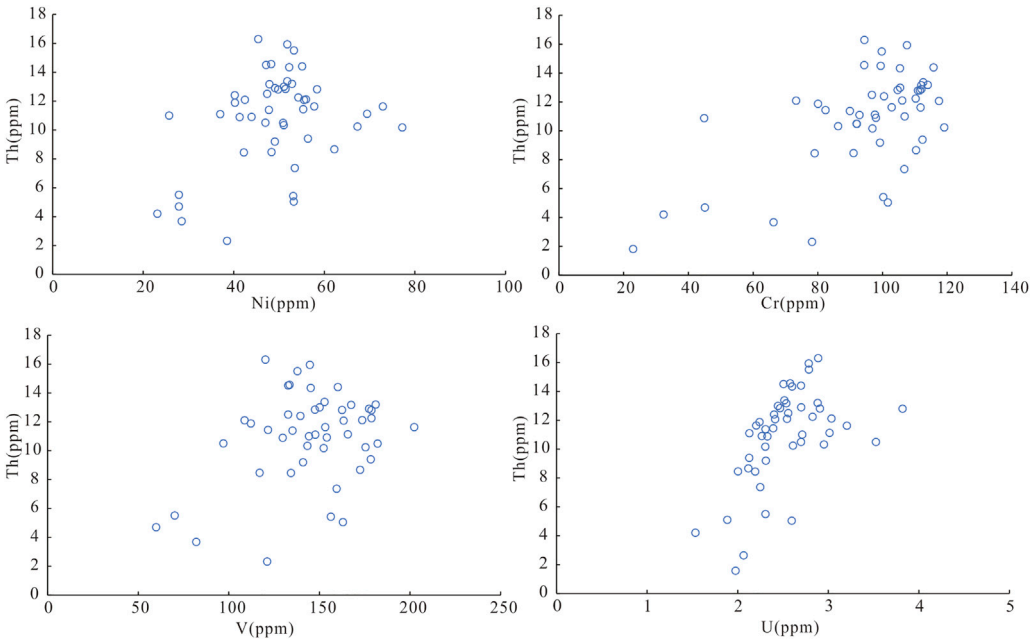

FIGURE 6
Binary cross-correlation plots of Th–Ni, Cr, V, and Th–U.

TABLE 1 Paleoclimate discrimination criteria based on the climate index (C) and chemical index of alteration (CIA) degree.

Climate index (*C*)	Chemical index of alteration (*CIA*)	Degree of chemical weathering	Paleoclimatic conditions
<.2	50–65	Low	Arid climate
.2–.6	65–85	Moderate	Semi-arid climate
>.6	85–100	Strong	Humid climate

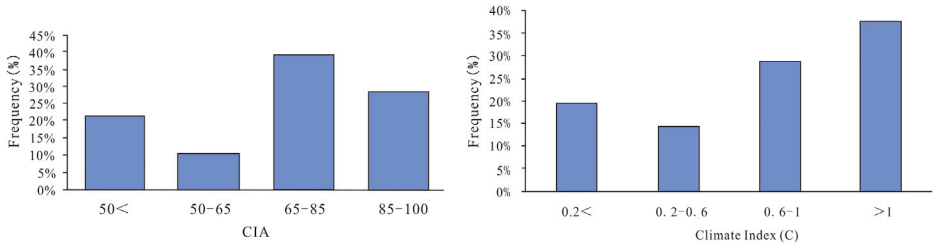

FIGURE 7
Frequency distribution of the chemical index of alteration (*CIA*) and climate index (*C*) for Well RA1.

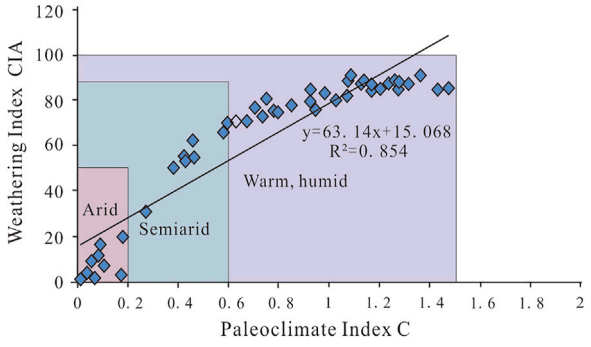

FIGURE 8
Distribution of climate Index (*C*) and chemical index of alteration (*CIA*) in the Da'anzhai Member of the Central Sichuan Basin.

Da'anzhai Member. The criteria for determining paleoclimate conditions are shown in Table 1. The defined paleoclimate indicator from Shi et al. (2022) is:

$$C - \text{value} = \sum(\text{Fe} + \text{Mn} + \text{V} + \text{Cr} + \text{Ni} + \text{Co}) \Big/ \times \sum(\text{Ca} + \text{Mg} + \text{Na} + \text{K} + \text{Sr} + \text{Ba}) \quad (2)$$

The analysis shows that the chemical index of alteration (*CIA*) of the shale samples from Well RA1 is distributed in the range of .96–90.87, with an average value of 63.02; most of the samples had *CIA* values above 65. The *CIA* of Well RA1 is also slightly lower than that of Well G10 which is located closer to the land source. The average *CIA* value of the Da'anzhai section of Well Gong 10 is 83 (Xiao et al., 2021). In addition, the paleoclimate index (*C*) for the shale samples from Well RA1 is distributed between .016 and .147, with an average value of .76 (Figure 7). A comprehensive analysis of the paleoclimate—based on both, the climate index (*C*) and chemical index of alteration (*CIA*), show that during the deposition of the Da'anzhai Member, most of the strata experienced moderate-to-strong chemical weathering in a semi-arid, warm and humid paleoclimate environment, and accompanied by a few episodes of dry paleoclimate conditions characterized by a lower weathering intensity (Figures 7, 8).

5.2 Evaluation of paleosalinity

Salinity is a good indicator of the environmental characteristics of a water body at any given time, and paleosalinity is the salinity of a water body at various times in geological history. Paleosalinity can be reproduced using paleontology, petrology, and isotope fractionation. The sedimentary environment of the Da'anzhai Member in the study area is very complex, and this study uses trace element content and ratio analysis to replicate its paleosalinity.

Recent studies report that the Da'anzhai Member in the Central Sichuan Basin was deposited in a typical continental freshwater lake basin environment, and that it experienced a complete sedimentary cycle of lacustrine transgression and regression (Xiao et al., 2021; Xu et al., 2022). The chemical properties of strontium (Sr) and barium (Ba) are similar, i.e. they can enter a solution in the form of soluble salts, and are very sensitive to changes in paleosalinity (Lin et al., 1999; Tribovillard et al., 2006; He et al., 2016). Strontium is more soluble than barium. With the increasing salinity of the formation water, Ba^{2+} will reach saturation first and precipitate as sulfates earlier than Sr^{2+}. Afterwards, as the salinity increases further, Sr^{2+} will precipitate. Therefore, a high Sr/Ba value reflects high paleo-salinity, and *vice versa*. A high Sr content also indicates an arid environment (Lin et al., 1999), consistent with high salinity aqueous media indicated by high Sr/Ba values. However, this indicator still has certain errors in the characterization of water salinity in continental lake basins. These errors are primarily because carbonate minerals tend to capture Sr and thus affect the

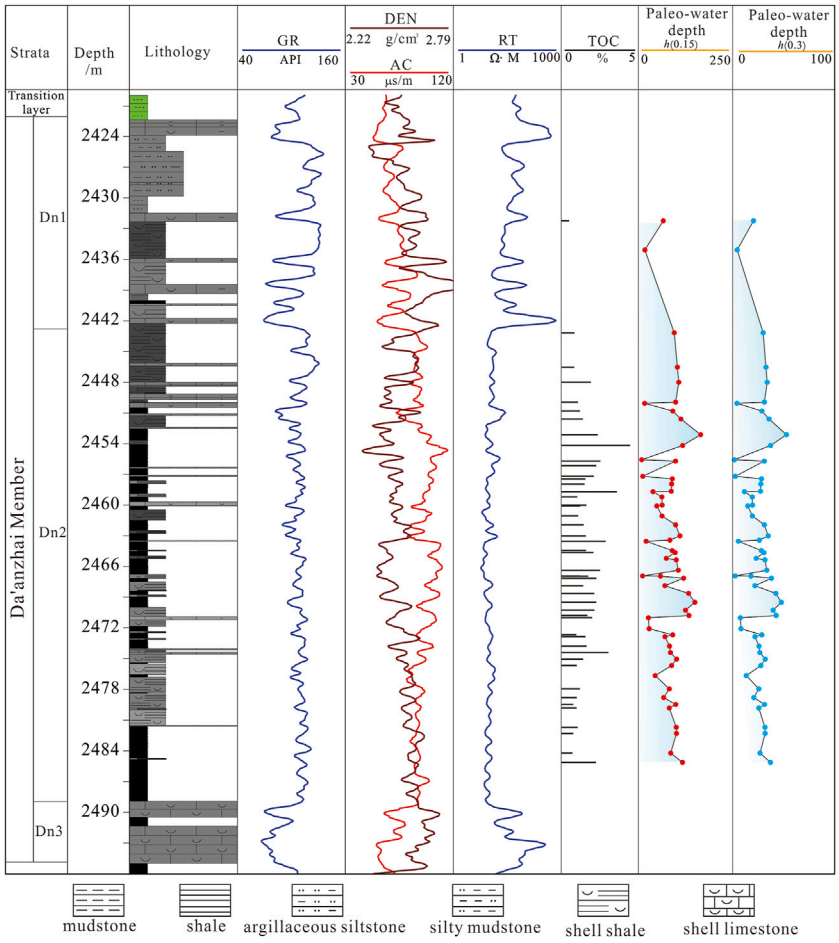

FIGURE 9
Vertical distribution of paleo-water depths in Well RA 1 in the Central Sichuan Basin; GR, gamma logging; DEN, Density Logging; AC, Acoustic logging; TOC, total organic carbon; Rt, True formation resistivity, Dn1, Dn2, Dn3: sub-members of the Da'anzhai member.

accuracy; Sr/Ba>1 is the salinization condition of lake water in marine or arid environments; 1>Sr/Ba>.5 is a brackish water phase; and Sr/Ba<.5 is the fresh water phase (Wu and Zhou, 2000).

The test results show that the Sr/Ba of the Da'anzhai Member of Well RA1 is .098–1.40, with an average value of .266. This indicates that the Da'anzhai Member of Well RA1 was deposited in a freshwater depositional environment, while a brackish water environment persisted periodically.

5.3 Evaluation of paleo-water depth

Shales developed in the Da'anzhai Member are generally considered to represent the semi-deep—deep lacustrine facies, but quantitative research on their genesis is lacking. In particular, there is no report on the paleo-water depth of the Da'anzhai Member based on geochemical methods. The calculation of paleo-water depths is based on the analysis of the mass fraction of cobalt (Co) in sedimentary rocks. This is a new method, which has achieved good results in practical applications (Wang X. J et al., 2022). In this paper, this method is used to estimate the water depth of the paleo-lake basin during the depositional period of the Da'anzhai Member of Well RA1. The formula from Wang X. J et al. (2022) is as follows:

$$V_s = V_o \times Nco/(Sco - t \times Tco) \quad (3)$$

$$h = 3.05 \times 10^5/(Vs1.5) \quad (4)$$

where h is the paleo-water depth, m; V_s is the deposition rate of the sample; V_o is the deposition rate of the normal lake at that time, 150–300 m/Ma; *Sco* is the cobalt abundance in the sample; *Nco* is the cobalt abundance in normal lake sediments, 20 (ppm); *Tco* is the cobalt abundance in the provenance, 4.68 (ppm); t is the cobalt contribution of the provenance to the sample (Fu et al., 2018). The distribution of rare Earth elements (REEs) in the upper crustal rocks is stable, so t can be replaced by ratio of lanthanum content of the samples to that of terrigenous clastic rocks (McLennan et al., 1993).

h(150) and h(300) are the paleo-water depth with deposition rates of 150 m/Ma and 300 m/Ma calculated from Eq. 4 respectively. The paleo-water-depth h(150) of Well RA1 ranges from 9.6 to 201.6 m, with an average value of 99.45 m; the paleo-water-depth h(300) is distributed between 3.4 and 71.3 m, with an average value of 35.16 m. This indicates that the Da'anzhai Member of Well RA1 was deposited

10.3389/feart.2022.1052734

TABLE 2 Relationship between lithofacies and sedimentary environment in Well RA1.

Lithofacies	Ancient water depth *h* (150)	Ancient water depth h (300)	Paleosalinity Sr/Ba	Climate *CIA*	Climate *SR/CU*	Redox (v/(v+Ni))	Ancient productivity	TOC (%)
Massive argillaceous shell limestone facies F	9.6–31.5	3.4–11.1	2.1–8.9	17.3–72.5	1.0–4.0	.21–.75	111.9–474.8	.5–1.2
Thick argillaceous shell limestone lithofacies E	30.5–34.0	10.8–12.0	.5–1.4	23.5–73.0	5.0–20.8	.75–.78	126.28–695.78	.72–1.2
Thin shell calcareous shale lithofacies C	24.0–109.0	8.5–38.5	.3–2.2	45.1–81.5	6.8–30.7	.67–.74	179.1–695.8	1.1–3.6
Laminar shell-bearing shale lithofacies B	58.8–201.7	20.8–71.3	.3–.8	50.1–80.2	5.0–98.8	.70–.79	542.3–1042.9	1.0–3.1
Thick siliceous shale A	75.8–182.9	26.8–64.7	.1–.4	49.5–79.7	5.4–44.9	.66–.78	457.2–1198.8	.7–4.5

in a semi-deep lake—shallow lake sedimentary environment (Figure 9).

5.4 Evaluation of paleoproductivity and paleo-oxidation reduction

Excess barium refers to barium derived from biological action, which is obtained by subtracting the Ba element in terrigenous debris from the total content of Ba element (Lin et al., 1999). It is calculated using the formula:

$$w(Baxs) = w(Ba)sample - w(Al)sample \times w(Ba)w(Al)PAAS \quad (5)$$

In the formula, (Ba)sample and (Al)sample are the mass fractions of Ba and Al in the tested sample, respectively; PAAS is a post-Archaean Australian shale (He et al., 2016). [w(Ba)/w(Al)]PAAS is the ratio of the mass fraction of Ba and Al elements in the shale samples, which is .0077.

When the calculated w(Baxs) value is greater than 1000 μg/g, the sedimentary system has a high paleoproductivity (He et al., 2016). The w(Baxs) values in Well RA1 range from 111.89 to 1,359.84 μg/g, with an average value of 630.71 μg/g. These results indicate that the Da'anzhai Member had poor paleoproductivity.

The redox-sensitive element ratios of fine-grained sediments have been widely used in the recovery of paleo-sedimentary environment identification (for example, V/Cr, V/(V+Ni), U/Th and δU). Compared with a single element, ratios of different elements have a strong anti-interference ability when judging ancient redox conditions. Thus, the stability of the calculation results is higher. Generally, in continental sedimentary basins, V/(V+Ni)>.5 represents anaerobic conditions, .5>V/(V+Ni)>.45 represents oxygen-poor conditions, and V/(V+Ni)<.45 represents oxygen-rich conditions. The result shows that the V/(V+Ni) difference in the Da'anzhai Member of Well RA1 is relatively obvious; its distribution ranges from .21 to .799, with an average value of .70. This feature indicates that the Da'anzhai Member of Well RA1 formed in an anaerobic depositional environment.

5.5 Evaluation of deposition rates

The deposition rate is a key factor that affects the production, degradation, and dilution of organic matter. Initially, the organic matter content increases with the deposition rate. When the deposition rate reaches a critical value, the organic matter starts to decrease despite the continuous increase of the deposition rate. A settling rate that is too low will cause the organics to degrade during the oxidation process, while a settling rate that is too high will dilute the organics. Analytically determining deposition rates are based on the analysis of element geochemistry, and the commonly used geochemical parameters are $(La/Yb)_N$, $(La/Yb)_N$ (Fu,2018). It represents the ratio of the La and Yb contents in the samples to the normalized values of the chondrites. La and Yb were used for the calculations because they represent LREE and HREE, respectively, and their content can be easily and accurately determined.

A lower deposition rate promotes the fractionation of fine-grained rare Earth elements when the suspended particles remain in the lake for a longer time. The rare Earth elements in the lake water

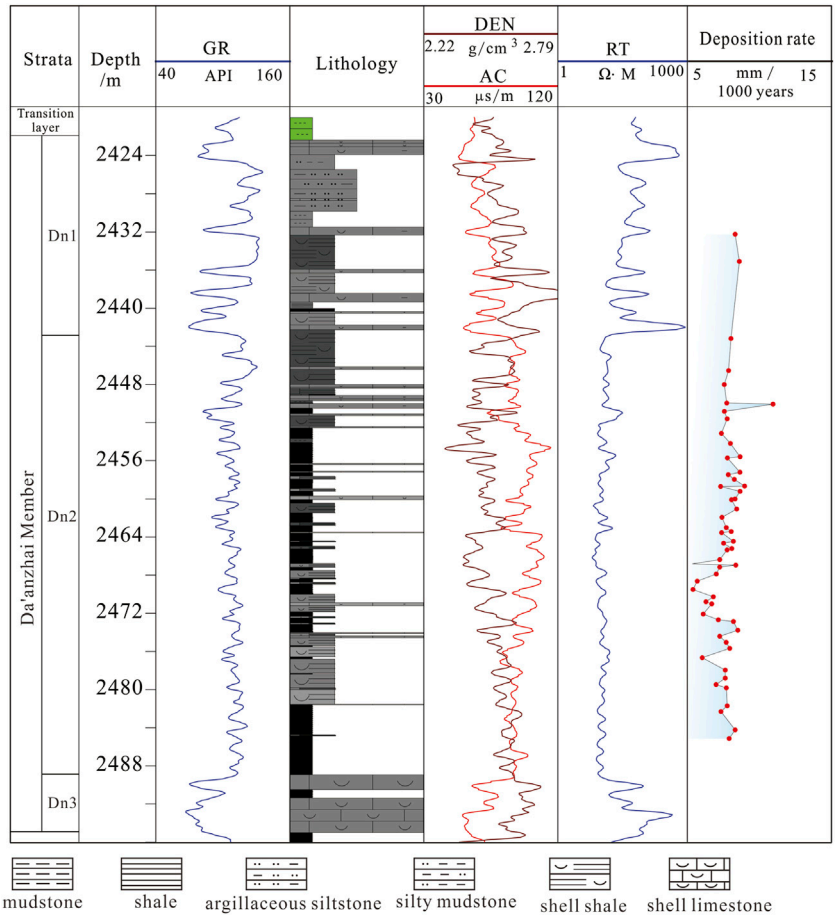

FIGURE 10
Vertical variation of sedimentation rates in Da'anzhai Member of Well RA1. GR, Natural gamma ray logging; AC, Acoustic logging; Rt, True formation resistivity logging, Dn1–Dn3: sub-member of Da'anzhai member.

have sufficient time to be adsorbed by the clay and react with the organic matter, which in turn leads to a significant differentiation of the rare Earth elements. In general, light rare earths are preferentially adsorbed by organic matter and clay fragments. They are converted into stable rare Earth complexes in lake water. A $(La/Yb)_N$ value of less than eight reflects a high deposition rate, and a $(La/Yb)_N$ value greater than ten reflects a low deposition rate.

The $(La/Yb)_N$ values of the samples in the study area range from 4 to 14 (Figure 10). This reflects a frequent change in the deposition rates. The $(La/Yb)_N$ value has a weak negative correlation with the TOC content, and the data points are scattered. It reflects three situations: 1) A lower deposition rate with the $(La/Yb)_N$ value greater than 10, and insufficient sediment supply and organic matter input. At this time, organic matter is easily degraded and oxidized, resulting in a lower TOC content; 2) A moderate deposition rate with the $(La/Yb)_N$ value between 8 and 10, and the organic matter input increases with increasing deposition rate; 3) A high deposition rate with the $(La/Yb)_N$ value less than 8, and an excessive deposition rate causes organic matter dilution. Therefore, the deposition rate when the $(La/Yb)_N$ value is between 8 and 10 is most favorable for the enrichment of organic matter. The $(La/Yb)_N$ value of the Da'anzhai Member ranges from 8 to 10, with an average value of 8.50. Here, the organic matter input increases with the deposition rate.

5.6 Influence of paleoenvironment on lithofacies

By comparing the evolution of the paleoenvironment and the distribution of lithofacies types (Table 2), it is found that different sedimentary paleoenvironmental conditions result in differences in rock characteristics (Zhang et al., 2015). Furthermore, it has a certain control on the distribution of lithofacies types.

In the sedimentary environment of continental lake basins, a change in the climate affects other paleoenvironmental elements to a large extent, which in turn affects the distribution characteristics of different types of lithofacies.

The arid climate lead to the reduction of water flow into the lake. This resulted in strong evaporation of the water body and its shallowing, and high salinity, low organic productivity, and the deposition of carbonate rocks with low TOC (Figure 11), such as lithofacies E and F (Table 2). Therefore, the major pore spaces of the lithofacies in arid climate are mostly intercrystalline pores (Figure 12).

Conversely, a warm and humid climate increased the volume of fresh water entering the lake. This inflow carried a large amount of terrigenous debris into the lake basin, increasing the content of quartz and feldspar in the sediment. A large amount of nutrients also entered the lake basin, which made organisms flourish, and the TOC in the

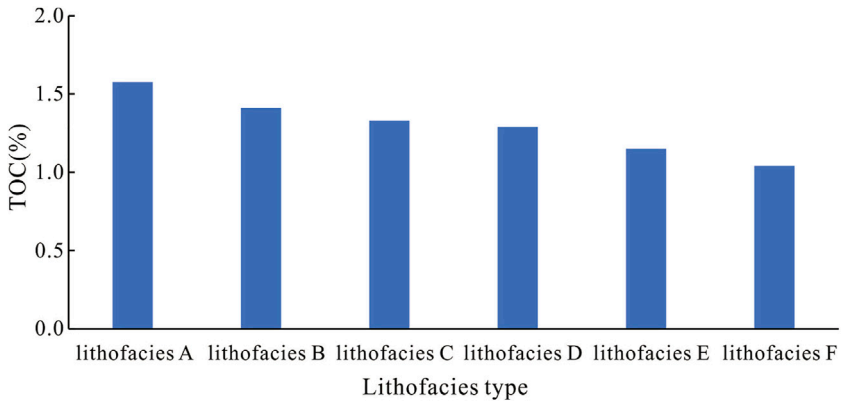

FIGURE 11
Average TOC content of each lithofacies type from Well RA1.

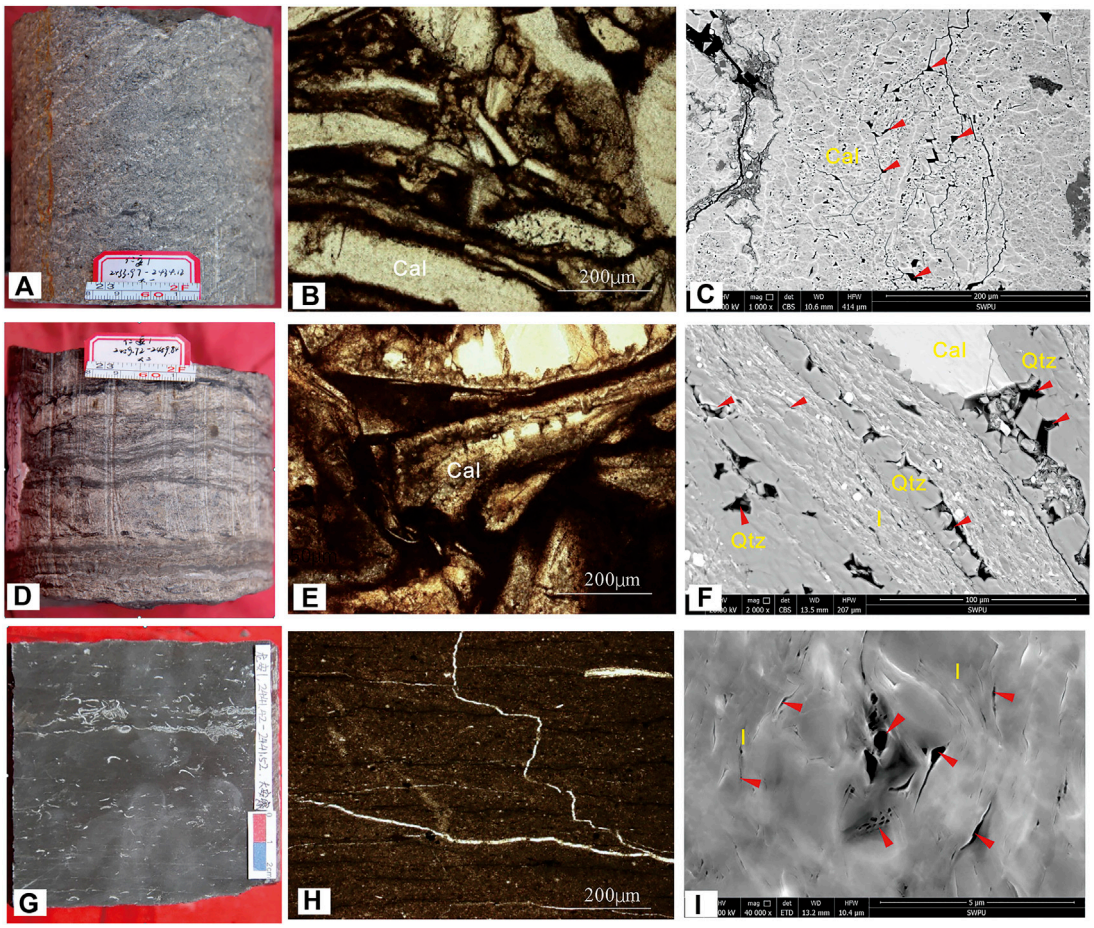

FIGURE 12
Core photographs of typical lithofacies and corresponding thin section microscopic image as well as pore characteristics under SEM of Well RA1. **(A)** massive mud-bearing shell limestone, 2,433.97–2,433.12 m; **(B)** microscopic photos of massive mud-bearing shell limestone, 2,433.97–2,433.12 m; **(C)** intercrystalline pores of shell calcite (Cal), 2,433.97–2,433.12 m; **(D)** medium-thick argillaceous shell limestone, 2,459.72–2,458.80 m; **(E)** microscopic photos of medium-thick argillaceous shell limestone, 2,459.72–2,458.80 m; **(F)** intercrystalline pores of quartz (Qtz) and clay minerals**(I)**, 2,459.72–2,458.80 m; **(G)** laminated shell-bearing shale, 2,441.42–2,441.52 m; **(H)** microscopic photos of laminated shell-bearing shale, 2,441.42–2,441.52 m; **(I)** intercrystalline pores of clay mineral **(I)**, 2,441.42–2,441.52 m.

sediments increase accordingly (Figure 11). Furthermore, the deepening of the water body reduced its salinity. This weakened the stratification of the water body and reduced the carbonate rock content. Multi-sedimentary mixed fine-grained sedimentary rocks were formed, such as facies A, B, C (Table 2) and the proportion of smaller pores, such as clay intercrystalline pores and organic pores increased (Figure 12).

When the overall climatic conditions remain unchanged, carbonate rocks are mostly developed in relatively shallow water environments. The deepening of the water body gradually decreases the volume of carbonate rocks being formed; mixed fine-grained sedimentary rocks gradually develop as well. Changes in the paleoenvironment and paleo-water medium conditions are direct reasons for the periodic prosperity and death of organisms; this provides sufficient organic matter. If the original productivity of the lake is certain, the reduced water medium environment is conducive to the preservation of organic matter. Organic matter is mostly decomposed under oxidative conditions.

The TOC content of fine-grained sedimentary rocks that form in relatively high salinity environments is usually high. This is because the water body is highly stratified under the conditions of a highly saline medium. The circulation between the surface water and the bottom water is blocked, forming a reducing environment at the bottom of the lake basin. A strong reducing environment is conducive to the preservation of organic matter. Regardless of gravity flow events, the content of the silt components in rocks will be affected to some extent by the depth of the water body and the supply of terrigenous debris. In a relatively shallow water environment, high terrigenous input resulted in the development of siltstone and silty fine-grained sedimentary rocks. With increasing distance from the shore and decreasing terrigenous input, the content of quartz and feldspar in the sediments also decrease accordingly.

6 Conclusion

1) The lithofacies of the Da'anzhai Member are divided into six types based on mineral composition, TOC and mineral structure—namely, massive mud-bearing shell limestone lithofacies (F), thick argillaceous shell limestone lithofacies (E), laminated clay silt shale lithofacies (D), thin shell calcareous shale lithofacies (C), laminated shell-bearing shale lithofacies (B), and thick clay shale lithofacies (A).
2) The pore types of the Da'anzhai Member include inorganic pores and organic pores. Inorganic pores are further classified into six sub-types including intergranular pores or intergranular dissolution pores in shell calcite, authigenic calcite intergranular pores, authigenic quartz intercrystalline pores, intergranular pores of clay minerals, and intergranular pores of pyrite nodules.
3) The Da'anzhai Member of Well RA1 was deposited in semi-deep to shallow lake sedimentary environment with relative low salinity and low organic productivity. During the deposition of the Da'anzhai Member, the strata were subjected to moderate-strong chemical weathering in semi-arid to warm and humid paleoclimate conditions. Weaker weathering and dry paleoclimate conditions occurred periodically.
4) The paleoenvironment was an important influence on the lithofacies and pore types of the Da'anzhai Member. The arid climate lead to a decline in water depth (Da1 and Da 3), which in turn resulted in relatively high salinity, low organic productivity, and the deposition of carbonate rocks that characterize lithofacies E and F. The major pore spaces of these carbonate rocks are mostly intercrystalline with comparatively larger radii. The warm and humid climate increased inflow of fresh water (Da2), terrigenous debris as well as nutrients into the lacustrine basin and led to the deposition of fine-grained sedimentary rocks (lithofacies A, B, C) which are characterized with abundant nano pores, such as clay intercrystalline pores and organic pores.

Data availability statement

The original contributions presented in the study are included in the article/supplementary material, further inquiries can be directed to the corresponding author.

Author contributions

RZ developed the idea for this paper and wrote the manuscript. BZ, MW, HAZ, SZ, WT, HOZ, YL, RB, MJ, and LH were involved in the logging interpretations.

Funding

This study was supported by a Science and Technology Cooperation project of the CNPC–SWPU Innovation Alliance (2020CX050103) and a National Natural Science Foundation of China grant (42202176).

Conflict of interest

Authors RZ, BZ, SZ, WT, HZ, YL, RB, MJ, YZ, and LH were employed by the PetroChina Southwest Oil & Gas Field Company.

The remaining authors declare that the research was conducted in the absence of any commercial or financial relationships that could be construed as a potential conflict of interest.

Publisher's note

References

Chen, S. J., Zhang, H. X., Lu, J. G., Yang, Y. M., Liu, C. W., Wang, L., et al. (2015). Controlling factors of Jurassic Da'anzhai Member tight oil accumulation and high production in central Sichuan Basin, SW China. *Petrol. explor. dev+.* 42 (2), 206–214. doi:10.1016/S1876-3804(15)30007-0

Curtis, J. B. (2002). Fractured shale-gas systems. *AAPG Bull.* 86 (11), 1921–1938. doi:10.1306/61EEDDBE-173E-11D7-8645000102C1865D

Fu, J. H., Li, S. X., Xu, L. M., and Niu, X. B. (2018). Paleo-sedimentary environmental restoration and its significance of chang 7 member of triassic yanchang formation in ordos basin, NW China. *Petrol. explor. Dev.* 45 (6), 998–1008. doi:10.1016/s1876-3804(18)30104-6

Fu, X. G., Wang, J., Zeng, S. Q., Feng, X. L., Wang, D., and Song, C. Y. (2017). Continental weathering and palaeoclimatic changes through the onset of the Early Toarcian oceanic anoxic event in the Qiangtang Basin, eastern Tethys. *Palaeogeogr. Palaeocl.* 487 (1), 241–250. doi:10.1016/j.palaeo.2017.09.005

Gao, Y., Huang, H., Tao, H., Carroll, A. R., Qin, J., Chen, J., et al. (2020). Paleoenvironmental setting, mechanism and consequence of massive organic carbon burial in the Permian Junggar Basin, NW China. *J. Asian Earth Sci.* 194 (1), 104222. doi:10.1016/j.jseaes.2019.104222

He, C., Ji, L., Wu, Y., Su, A., and Zhang, M. (2016). Characteristics of hydrothermal sedimentation process in the Yanchang Formation, south Ordos Basin, China: Evidence from element geochemistry. *Sediment. Geol.* 345, 33–41. doi:10.1016/j.sedgeo.2016.09.001

Huang, D., Duan, Y., Li, Y. C., Chen, H. B., Yan, W. P., and Dai, H. M. (2018). Study on the lower limit of organic carbon content in freshwater lacustrine shale oil and gas: A case study of daanzhai section of jurassic in Sichuan Basin. *China Petrol. explor.* 23 (6), 38–45. doi:10.3969/j.issn.1672-7703.2018.06.005

Huo, F., Wen, H. G., Li, L., Luo, B., Zhou, G., Xu, W. L., et al. (2022). Influence of the depositional environment on the formation of organic-rich marine shale: A case study of the first discovery of anisian shale in the Sichuan Basin. *J. Pet. Sci. Eng.* 214, 110577. doi:10.1016/j.petrol.2022.110577

Krom, M. D., and Berner, R. A. (1983). A rapid method for the determination of organic and carbonate carbon in geological samples. *J. Sedi. Res.* 53 (2), 660–663. doi:10.1306/212F8260-2B24-11D7-8648000102C1865D

Lei, W., Chen, D., Zhang, R., Liu, Z. Y., and Zhang, S. M. (2021). Lithological combination types and characteristics of continental shale strata in the second submember of Da'anzhai in central sichuan. *Earth Sci.* 46 (10), 3657–3672. doi:10.3799/dqkx.2021.023

Li, H., Tang, H. M., Qin, Q. R., Zhou, J. L., Qin, Z. J., Fan, C. H., et al. (2019). Characteristics, formation periods and genetic mechanisms of tectonic fractures in the tight gas sandstones reservoir: A case study of xujiahe formation in YB area, Sichuan Basin, China. *China. J. Petrol. Sci. Eng.* 178, 723–735. doi:10.1016/j.petrol.2019.04.007

Li, H., Zhou, J. L., Mou, X. Y., Guo, H. X., Wang, X. X., An, H. Y., et al. (2022). Pore structure and fractal characteristics of the marine shale of the longmaxi formation in the changning area, southern Sichuan Basin, China. *Front. Earth Sci.* 10, 1018274. doi:10.3389/feart.2022.1018274

Li, Y. Q., and He, D. F. (2014). Early Jurassic tectonic sedimentary environment and prototype basin evolution in Sichuan Basin and its adjacent areas. *Acta. Petrol. Sin.* 35 (2), 219–232. doi:10.7623/syxb201402002

Lin, H. L., Lai, C. T., Ting, H. C., Wang, L. J., Michael, S., and Huang, J. J. (1999). Late pleistocene nutrients and sea surface productivity in the south China sea: A record of teleconnections with northern hemisphere events. *Mar. Geol.* 156 (1), 197–210. doi:10.1016/S0025-3227(98)00179-0

Liu, S. G., Deng, B., Li, Z. W., and Sun, W. (2012). Architecture of basin-mountain systems and their influences on gas distribution: A case study from the Sichuan Basin, south China. *J. Asian Earth Sci.* 47, 204–215. doi:10.1016/j.jseaes.2011.10.012

McLennan, S. M., Hemming, S., McDaniel, D. K., and Hanson, G. N. (1993). Geochemical approaches to sedimentation, provenance, and tectonics. *Geol. Soc. Am. Special Pap.* 284, 21–40. doi:10.1130/SPE284-p21

Meakin, P., Huang, H., Malthe-Sorenssen, A., and Thogersen, K. (2013). Shale gas: Opportunities and challenges. *Environ. Geosci.* 20 (4), 151–164. doi:10.1306/eg.05311313005

Michaelis, W., Seifert, R., Nauhaus, K., Treude, T., Thiel, V., Blumenberg, M., et al. (2002). Microbial reefs in the black sea fueled by anaerobic oxidation of methane. *Science* 297 (5583), 1013–1015. doi:10.1126/science.1072502

Milliken, K. (2014). A compositional classification for grain assemblages in fine-grained sediments and sedimentary rocks. *J. Sediment. Res.* 84 (12), 1185–1199. doi:10.2110/jsr.2014.92

Nesbitt, H. W., and Young, G. M. (1989). Formation and diagenesis of weathering profiles. *J. Geol.* 97 (2), 129–147. doi:10.1086/629290

Pang, Z. L., Tao, S. Z., Zhang, Q., Yang, J. J., Zhang, T. S., Yang, X. P., et al. (2018). Reservoir micro structure of Da'anzhai member of jurassic and its petroleum significance in central Sichuan Basin, SW China. *Petrol. explor. dev+.* 45 (1), 68–78. doi:10.1016/s1876-3804(18)30006-5

Shi, J. Z., Cui, H. F., Xu, W., Song, B., and Wang, B. W. (2022). Sedimentary environment and organic matter enrichment model of black shale from cretaceous bayingebi formation in balongwula, yingen-ejin banner basin. *Geol. Bull. China* 41 (8), 1430–1444. doi:10.12097/j.issn.1671-2552.2022.08.010

Su, K. M., Lu, J. G., Zhang, G. W., Chen, S. J., Li, Y., Xiao, Z. L., et al. (2018). Origin of natural gas in jurassic Da'anzhai member in the Western part of central Sichuan Basin, China. *J. Petrol. Sci. Eng.* 167, 890–899. doi:10.1016/j.petrol.2018.04.014

Tribovillard, N., Algeo, T. J., Lyons, T., and Riboulleau, A. (2006). Trace metals as paleoredox and paleoproductivity proxies: An update. *Chem. Geol.* 232 (1–2), 12–32. doi:10.1016/j.chemgeo.2006.02.012

Wang, C. Y., Chang, J., Li, N., Hong, H. T., Li, Y. N., Wang, X. J., et al. (2022). Paleo-water-depth reconstruction of early jurassic lakes in the eastern Sichuan Basin. *Acta. Petrol. Sin.*, 1–16. doi:10.14027/j.issn.1000-0550.2022.036

Wang, S. F., Dong, D. Z., Wang, Y. M., Li, X. J., Huang, J. L., and Guan, Q. Z. (2016). Sedimentary geochemical proxies for paleoenvironment interpretation of organic-rich shale: A case study of the lower silurian longmaxi formation, southern Sichuan Basin, China. *J. Nat. Gas. Eng.* 28, 691–699. doi:10.1016/j.jngse.2015.11.045

Wang, W., Huang, D., Yi, H. Y., Zhao, R. R., Cen, Y. J., and Li, Y. C. (2019). Fine division and geochemical characteristics of freshwater lacustrine shale sublayers: A case study of daanzhai member of jurassic in Sichuan Basin. *Petrol. Geol. Expt.* 41 (5), 724–730. doi:10.11781/sysydz201905724

Wang, X. J., Zhou, Y. S., Peng, J., Li, J., Li, H. L., Wang, Y. M., et al. (2022). Major breakthrough of shale gas in the jurassic qianfoya formation in puguang area in the northeastern Sichuan Basin. *China Petrol. explor.* 27 (5), 52–61. doi:10.3969/j.issn.1672-7703.2022.05.005

Wu, Z. P., and Zhou, Y. Q. (2000). A new method to calculate the deposition rate -- the characteristic element method of cosmic dust. *J. Depos.* 18 (3), 395–399. doi:10.14027/j.cnki.cjxb.2000.03.012

Xiao, Z. L., Chen, S. J., Zhang, S. M., Zhang, R., Zhu, Z. Y., Lu, J. G., et al. (2021). Sedimentary environment and model for lacustrine organic matter enrichment: Lacustrine shale of the early jurassic Da'anzhai formation, central Sichuan Basin, China. *J. Palaeogeog.* 10 (4), 584–601. doi:10.1016/j.jop.2021.09.002

Xu, Q., Liu, B., Song, X. M., Wang, Q. P., Chen, X. D., Li, Y., et al. (2022). Hydrocarbon generation and organic matter enrichment of limestone in a lacustrine mixed sedimentary environment: A case study of the jurassic Da'anzhai member in the central Sichuan Basin, SW China. *Petrol. Sci.* doi:10.1016/j.petsci.2022.10.002

Yang, X. P., Zou, C. N., Tao, S. Z., Wang, Z. C., Li, J., and Wang, S. Q. (2005). Characteristics of upper triassic-jurassic oil and gas system in Sichuan Basin and oil and gas abundance law. *China Pet. Explor* 10 (2), 15–22. doi:10.3969/j.issn.1672-7703.2005.02.003

Zhang, S., Chen, S. Y., Yan, J. H., Tan, M. Y., Zhang, Y. Y., Gong, W. L., et al. (2015). Characteristics of shale lithofacies and reservoir space in the 3rd and 4th members of Shahejie Formation, the west of Dongying Sag. *Nat. Gas. Geosci.* 26 (2), 320–332. doi:10.1176/j.issn.1672-1926.2015.02.0320

Zheng, R. (2014). High resolution sequence stratigraphy of Da'anzhai formation, lower jurassic in Sichuan Basin. *Acta. Petrol. Sin.* 16 (2), 42–49. doi:10.14027/j.cnki.cjxb.1998.02.009

Zhou, G. Z., Hu, Z. M., Liu, X. G., Wu, J. F., Chang, J., and Chen, X. K. (2021). Palaeoenvironmental analysis of the lower silurian longmaxi formation in the zhaotong area of the Sichuan Basin, south China: Implications for organic matter accumulation mechanisms. *Geol. J.* 56 (3), 1358–1381. doi:10.1002/gj.3934

Zhou, Y., Yang, F. L., Ji, Y. L., Zhou, X. F., and Zhang, C. H. (2020). Characteristics and controlling factors of dolomite karst reservoirs of the Sinian Dengying Formation, central Sichuan Basin, southwestern China. *Precambrian Res.* 343, 105708. doi:10.1016/j.precamres.2020.105708

Zhu, H. H., Chen, L., Cao, Z. L., Wang, M. L., Hong, H. T., Li, Y. C., et al. (2022). Microscopic pore characteristics and controlling factors of black shale in the Da'anzhai Member of Jurassic Ziliujing Formation, central Sichuan Basin. *Oil Gas Geol.* 43 (5), 1115–1126. doi:10.11743/ogg20220509

Zhu, H. H., Zhang, T. S., Liang, X., Zhang, Z., and Zhang, L. (2018). Insight into the pore structure of Wufeng-Longmaxi black shales in the south Sichuan Basin, China. *J. Petrol. Sci. Eng.* 171, 1279–1291. doi:10.1016/j.petrol.2018.08.061

Zou, C. N., Dong, D. Z., Wang, S. J., Li, J., Li, X., Wang, Y., et al. (2010). Geological characteristics and resource potential of shale gas in China. *Petrol. explor. dev+.* 37 (6), 641–653. doi:10.1016/S1876-3804(11)60001-3